metals

MDPI

Article

First-Principles Study on Silicon Stabilization of the Cubic α- and Hexagonal α′-FeAl Phases

Changming Fang *, Zhongping Que and Zhongyun Fan

Brunel Centre for Advanced Solidification Technology (BCAST), Brunel University London, Uxbridge UB8 3PH, UK; zhongping.que@brunel.ac.uk (Z.Q.); zhongyun.fan@brunel.ac.uk (Z.F.)
* Correspondence: changming.fang@brunel.ac.uk

Abstract

Commercial aluminum (Al) metals contain unavoidable impurities, such as iron (Fe) and silicon (Si). Due to its low solubility and high chemical affinity to Al, Fe exists in the form of Fe-containing intermetallic compounds (Fe-IMCs), which are crucial in solidification processes, determining the micro-structure and consequently the mechanical performance of the cast parts. Meanwhile, Si, as an impurity or addition, may join the binary Fe-IMCs. Here, we investigate the Si stabilization effects on the frequently observed Al-rich Fe-IMCs in a comprehensive and systematic way using a first-principles density-functional theory (DFT) approach. The study reveals different Si stabilization effects on the cubic α- and hexagonal α′-phase, as well as other binaries: $Al_{12}Fe$, η-Al_6Fe, τ_4-, β-, and θ-phases. The enhancement of stability for the α-phase is moderate, while it is strong for the α′-phase. For the stability series (from higher to lower) is θ-$Al_{13}Fe_4$ > η-Al_6Fe > α-$Al_{4.75}Fe$ in the binary system, while it becomes τ_4-$(Al,Si)_5Fe$ > β-$Al_{4.5}SiFe$ > α′-$(Al,Si)_{4.174}Fe$ for the ternary Fe-IMCs. The information obtained here helps understand the formation of Fe-IMCs particles during casting of Al-Si alloys, and the design of novel Al alloys of fine micro-structures and desired mechanical performances of the products from the primary Al and the scraps and wastes.

Keywords: Si stabilization; Fe-containing intermetallic compounds; cubic α-phase; hexagonal α′-phase; first-principles calculations; density-functional theory

1. Introduction

Commercial Al metals contain unavoidable impurities, including iron (Fe) and silicon (Si). The low solid solubility of Fe (less than 0.05 wt.%) at equilibrium in solid Al and its high affinity to Al [1,2] drive it to form Fe-containing intermetallic compounds (Fe-IMCs) in aluminum-based alloys [2,3]. Si is frequently added to Al metals for improving castability, refining microstructures, and enhancing the mechanical properties of the cast parts [3,4]. The Si impurity or addition may join the binary AlFe compounds to produce ternary Fe-IMCs. The Fe-IMCs particles formed during casting exhibit various morphologies and may deteriorate the mechanical performance of the products. Such a deterioration effect becomes more severe for recycling of Al scraps/wastes in which various Fe-IMCs particles would have been accumulated during usage, storage, and treatments [5–8]. Various methods, including separating the heavier Fe-IMCs particles from the liquids [9,10], manipulating solidification processes and/or adding minor elements to transform the detrimental Fe-IMCs into less harmful or even beneficial nano-sized particles [11–14] have been explored. Reaching such aims means demanding a systematic and comprehensive understanding of the crystal chemistry of the Al-rich Fe-IMCs, which helps manipulate the formation of the

Academic Editors: Xiangyuan (Carl) Cui, Zhengyi Jiang and Andrii Kostryzhev

Received: 12 May 2026
Revised: 25 June 2026
Accepted: 8 July 2026
Published: 30 July 2026

Fe-IMCs in various Al ingots, including Al-scraps/wastes, which contain various contents of Fe and Si [1,10,11]. The latter is important for our environment and the increasingly important recycling economy [15–17].

Currently, experiments focus on alloy manufacturing, micro-structural analysis, phase characterizations [1–4,7,9,12–14,18–21], and mechanical properties measurements [21–23]. Moreover, great efforts have been made to determine the crystal structures of these Al-rich Fe-IMCs. Structural models were built for the η-Al_6Fe [24], τ_4- [25,26], β- [27–29], cubic α- [30], hexagonal α′- [31,32], and θ-phase [33] based on dominantly X-ray-diffraction patterns and structural refinements. For most ternary Fe-IMCs, the structural determination generally provided 'averaged' patterns in which the Al/Si atoms were assumed to be uniformly distributed at the Wyckoff sites of the Al atoms. One example is in the cubic α-(AlFeSi) phase [30]. Moreover, there are partial atomic occupations at the specific Wyckoff sites in, e.g., the hexagonal α′-(AlFeSi) phase [31,32]. Al/Si distribution often complicates our understanding of their thermodynamic properties under solidification conditions and the mechanical performance of the produced alloys in practice.

In this respect, atomistic modeling methods, particularly parameter-free ab initio/first-principles approaches, become helpful. First-principles approaches can assist in building structural models and predicting intrinsic structural properties for complex compounds [34,35]. First-principles density-functional theory (DFT) approaches have been applied to the Fe-IMCs-related materials [36–44]. Wolverton and Ozolins [36] constructed an energetic database for a series of binary Al-containing alloys and compounds, including several Fe-IMCs, with the help of DFT methods. Liu et al. reported the results of their first-principles study on the mechanical properties and electronic structures of several binary Fe-IMCs [37]. The Al/Si ordering in the β-AlFeSi phase was investigated using an electronic DFT method [38,39]. Popčevič et al. investigated the electronic and magnetic properties of θ-$Al_{13}Fe_4$ phase [40]. Ma studied the mechanical and electronic properties of α-AlMnSi [41]. Zhang et al. performed first-principles modeling on the Fe/Mn occupation in α-AlMnFeSi [42]. Amirkhanyan et al. studied the stability and lattice vibrations of the τ_4-phase [43]. The Si occupation at the Al sites in the Fe-IMCs, including η-Al_6(Mn,Fe) alloying phase [44], β- [45], τ_4-phase [46], and θ-$Al_{13}Fe_4$ [44,47,48], as well as the cubic α-Al(Fe,Mn) phase [49], was investigated by means of first-principles tools. Meanwhile, there is still a lack of comprehensive understanding about structural models and Si occupations in the ternary cubic α- and hexagonal α′-phase, together with other binary Fe-IMCs.

It is noted that in the Al-Fe binary phase diagram, θ-$Al_{13}Fe_4$ is the stable phase in the Al-rich region (x(Fe) < 24.0 at%), and other Fe-IMCs, including the cubic α- and hexagonal α′-phase, are non-existent under ambient conditions [2,22]. Therefore, the above-mentioned binary cubic α- and hexagonal α′-AlFe phases are hypothetical. Meanwhile, the experiments revealed that the cubic α-particles were formed in Si-poor Al alloys, and the hexagonal α′-phase was formed in Al-alloys with relatively high Si content [1,4,19]. Here, we investigate the structure chemistry of the novel/hypothetical binary α- and α′-phase starting from the available experimental models [30–32]. This study also includes the Si stabilization effects on other frequently observed Fe-IMCs, such as (novel) $Al_{12}Fe$, (novel) η-Al_6Fe, τ_4-$(Al,Si)_5Fe$, β-$Al_{4.5}SiFe$, and θ-$(Al,Si)_{13}Fe_4$ phases. This produces a systematic and comprehensive understanding of their stability and the related Si stabilization effects on these Al-rich Fe-IMCs. The information obtained here is useful to design new casting processes and new Al alloys from both primary Al billets and scraps/wastes.

2. Methods

The stability of one Fe-IMC with the chemical formula $Al_kSi_mFe_n$ can be referred to the related elemental solids. Therefore, its formation energy (ΔE_f) is defined as:

$$\Delta E_f(Al_kSi_mFe_n) = \{E(Al_kSi_mFe_n) - [k\,E(Al) + m\,E(Si) + n\,E(Fe)]\}/n \quad (1)$$

Here, $E(Al_kSi_mFe_n)$, $E(Al)$, $E(Si)$, and $E(Fe)$ represent the calculated total valence-electron energies for $Al_kSi_mFe_n$ and the elemental solids, α-Al, Si, and α-Fe, respectively. The unit of the formation energy, ΔE_f, is eV per Fe atom.

In order to assess the Si stabilization effects on the binary Fe-IMCs, the formation energy of the Si joined the compound $Al_kSi_mFe_n$ in its unit cell is defined as:

$$\Delta E_{Si}(Al_kSi_mFe_n) = E(Al_kSi_mFe_n) - \{E(Al_{(k+m)}Fe_n) + m\,[(E(Si) - E(Al)]\} \quad (2)$$

Here, $E(Al_{(k+m)}Fe_n)$ represents the total valence-electrons energy for $Al_{(k+m)}Fe_n$. The unit of formation energy in Equation (2) is eV per cell.

Considering the Fe-IMCs with various Al(Si)/Fe ratios, the formation energy of a Si-joined compound, $Al_kSi_mFe_n$, is unified into eV/Fe as follows:

$$\Delta E_{Si2}(Al_kSi_mFe_n) = \Delta E_{Si2}(Al_kSi_mFe_n)/n \quad (3)$$

A negative value of the formation energy in the Equations means that the reaction is exothermic, and the formation of the compound is favored.

The first-principles Vienna Ab initio Simulation Package (VASP) [50] was employed in the present study. This code utilizes the density-functional theory (DFT) [51] within the projector-augmented wave (PAW) method [52]. The spin-polarized generalized gradient approximation (GGA) formulated by Perdew, Burke, and Ernzerhof (PBE) [53] was used for the exchange and correlation energy terms, as the GGAs describe the 3D metals, including Fe and its related compounds, better than the local (spin-polarized) density approximation [53,54].

The cut-off energies for the wave functions and for the augmentation functions were set to be 550.0 eV and 700.0 eV, respectively. These cut-off energies are notably higher than the default values (E_{MAX}/E_{AUG} = 245.3 eV/322.1 eV for Si, 240.3 eV/291.1 eV for Al, and 267.9 eV/511.4 eV for Fe, respectively) in the atomic pseudo-potentials. The electronic wave functions were sampled densely on, for example, a 6 × 6 × 6 grid with 11 to 108 ***k***-points in the irreducible Brillouin zones of the cubic α-$(Si_{1-x}Al_x)_{114}Fe_{24}$ phase, depending on the symmetry, using the Monkhorst–Pack method [55]. Structural optimizations were performed for both lattice parameters and the coordinates of atoms. Different ***k***-meshes and cut-off energies were tested, which showed a good convergence with deviations within 1 meV/atom.

3. Results

First-principles structural optimizations were first performed for the related elemental solids, Al, Si, and Fe, all of which have cubic lattices. The calculations produced a lattice parameter of 4.039 Å (4.0493 Å) for α-Al, 5.468 Å (5.431 Å) for Si, and 2.829 Å (2.8665 Å) for α-Fe. These calculated values agree well with the experimental data at room temperature [56] (see the values in parentheses). The calculations provided a ferromagnetic solution for α-Fe, which contains $3d^6$ electrons. The obtained local moment is moderate (2.17 μ_B/Fe), which is close to the experimental value (2.22 μ_B/Fe) [57]. The excellent agreement between the experimentally measured values and the calculations means the approach and settings are valid.

The calculations also showed that the Fe solution in the Al matrix, which was modeled in a $3a_0 \times 3a_0 \times 3a_0$ supercell, a_0 being the lattice of Al, and thus the formula was $Al_{107}X$, X = Fe or Si, is favored with the formation energy of −0.45 eV/Fe. Meanwhile, the solution

of Si in the Al matrix costs energy (+0.43 eV/Si) (Table 1). The bond lengths between the impurities and the surrounding Al atoms are 2.74 Å (Fe-Al) and 2.84 Å (Si-Al), respectively. These values are shorter than the Al-Al bond (2.86 Å) in α-Al.

Table 1. The calculations for the binary α- (cubic) and α'-AlFe (hexagonal) models based on the experimental determinations, whose values are in the parentheses [30], or specifically labeled [31,32]. FCC/BCC represents face-centered cubic/body-centered cubic. The unit of the diluted Fe in the Al matrix and the formation energies of the compounds, ΔE_{f1}, are eV/Fe via Equation (1).

Phase	Lattice/Space Group	Latt. Parameters (Å)	$E_{\text{val.-elect.}}$	Remark
A. Solute Fe and Si in Al matrix				
$Al_{107}Fe$	-	-	−0.449 (eV/Fe)	d (Fe-Al):2.74 Å (×12)
$Al_{107}Si$	-	-	+0.431 (eV/Si)	d (Si-Al): 2.84 Å (×12)
B. Cubic α-AlFe with space group P-3m (200) Cooper [30]				
α-$Al_{114}Fe_{24}$	Cub. PM-3 (No. 200)	a =12.622 (12.56) [30]	−1.315 (eV/Fe)	Based on [30]
C. Hexagonal α'-AlFe with space group $P6_3/mmc$ (194), 607475-ICSD, Corby–Black [31]				
Config-1 $Al_{194}Fe_{46}$	Hex./$P6_3/mmc$ (194)	a = 12.450 (Å) c = 26.393 (Å)	−1.301 (eV/Fe)	Al17 are removed
Config-2 $Al_{192}Fe_{46}$	Hex./$P6_3/mmc$ (194)	a = 12.446 (Å) c = 26.374 (Å)	−1.289 (eV/Fe)	Al17 and Al18 are removed
Config-3 $Al_{188}Fe_{46}$	Hex./$P6_3/mmc$ (194)	a = 12.380 (Å) c = 26.349 (Å)	−1.239 (eV/Fe)	Al17 and Al14 are removed
Config-4 $Al_{186}Fe_{46}$	Hex./$P6_3/mmc$ (194)	a = 12.379 (Å) c = 26.225 (Å)	−1.250 (eV/Fe)	Al17, Al14 and Al18 are removed
Exper. $Al_{192–194}Fe_{46}$	Hex./$P6_3/mmc$ (194)	a = 12.404 (Å) [31] c = 26.234 (Å) [31] a = 12.3445 (Å) [32] c = 26.210 (Å) [32]	-	Al16/Al17 mixing, Al18 small occup. Symmetry of the crystal is broken.

3.1. Structure of the Binary α- and α'-AlFe Phases

As mentioned before, in the binary Al-Fe phase diagram, both cubic α- and the hexagonal α'-AlFe are non-existent [22,23]. In order to obtain detailed information about Si occupation at the Al sites in the structures, we assumed that all the Al/Si sites were occupied by Al as the starting point. Consequently, we built hypothetical structures for the binary cubic α- and the hexagonal α'-AlFe based on the available experimental structures of the ternary compounds [30–32].

Cooper determined the crystal structure of the cubic α-(AlFeSi) crystals, which contained an amount of Mn [30]. He proposed three models with fully Al-occupied Wyckoff sites, based on the X-ray diffraction patterns. The models avoid partial occupations and keep the symmetry of the systems [30]. Structural refinements provided similar values of refinement goodness for the three models. The atomic coordinates and related occupations for Model 3 in [30] are listed in the Supplementary Materials (Table S1) with the labels of the atom sites. The unit cell contains 138 atoms with the chemical formula $Al_{114}Fe_{24}$.

First-principles calculations were performed for the three models and revealed similar formation energies. The results of structure optimizations for the cubic α-AlFe phase (Model 3) are shown in Table 1.

The crystal structure of the hexagonal α′-(AlFeSi) phase was experimentally investigated for a long time [31,32,58]. Corby and Black determined the crystal structure of the hexagonal α′-(AlFeSi) phase by means of the anomalous-dispersion methods with three different wavelengths of radiation on a single crystal [31]. The crystal structure of α′-(AlFeSi) has a space group of $P6_3/mmc$ (194) and lattice parameters, a = 12.404 (Å) and c = 26.234 (Å) [31]. There are 23 different atomic Wyckoff sites, five Fe sites, and 18 Al sites. The Si atoms were assumed to be homogeneously distributed at the Al sites. There are partial occupations at the Al/Si sites [31]. Roger et al. [32] refined the crystal structure of α′-(AlFeSi) and obtained lattice parameters slightly different from those in [31], as shown in Table 1. Moreover, the Al and Si separately occupied sites were reported [32]. The atomic coordinates and related occupations are listed in the Supplementary Materials, Table S2 for both the Corby–Black model [31] and the Roger model (CSD-422224) [32]. Table S2 also includes the labels of the atomic Wyckoff sites. If we take full occupation of all Al sites, the chemical formula is α′-$Al_{200}Fe_{46}$. However, this model contains short interatomic distances between Al16 and Al(Si)17 with a short Al-Al(Si) distance (<0.5 Å), which means there is partial occupation at the two sites. Therefore, the occupation of either Al16 or Al17 should be chosen to keep system symmetry. Moreover, the occupation of the Al(Si)18 (2c) sites is small (0.14 [32] or 0.29 [31]). The experimental structural model is 'averaged', and the symmetry is practically broken.

Based on the structural model [31,32], we performed first-principles calculations for configurations with Al vacancies at the Al sites and found the ones with low energy costs, as shown in Table 1. We calculated configurations with an Al vacancy either at the Al16 site or the Al17 site and revealed the same formation energy. The results for Al vacancies at the Al17 site, with the chemical formula $Al_{194}Fe_{46}$, for the configurations are shown in Table 1.

As shown in Table 1, the calculated lattice parameter for the cubic α-$Al_{114}Fe_{24}$ is 12.622 Å, which is close to the experimental value for the ternary compound (12.56 Å) [30]. The calculated formation energy is −1315 meV/Fe.

The hexagonal α′-phase with the maximum Al content has the chemical formula $Al_{194}Fe_{46}$ (Config-1 in Table 1) with a formation energy of −1301 meV/Fe. This α′-$Al_{194}Fe_{46}$ is obtained by removing either the Al16 or Al17 atoms. We also performed structural optimizations and total energy calculations for configurations with Al vacancies at mixing Al16/Al17, in which system symmetry is broken. The calculations produced the same formation energy within the numeric errors as that of Config-1.

Decreasing the number of Al atoms in the unit cell of α′-phase induces an increase in the formation energies (Table 1). When the atoms at both Al17 and Al18 were removed, the formation energy of α′-$Al_{192}FeSi_{46}$ (Config-2) is −1289 meV/Fe, just slightly lower than that of Conf-1. This configuration was selected for the study of the Si stabilization effect, considering the moderate occupation at Al(Si)18 [31,32]. Further removing Al atoms at other sites, e.g., Al14, causes a notable decrease in the stability of the systems.

3.2. Si Stabilization Effect on the Cubic α-$FeAl_{4.75}$ Phase

Table 1 showed that the crystal structure of the α-(AlFeSi) phase has a cubic lattice (space group Pm-3, Nr. 200) [30]. There are two types of iron sites which are labeled as Fe1 at 12j and Fe2 at 12k Wyckoff sites and nine Al sites at 6e (Al1), 6h (Al2), 12j (Al3), 12k (Al4), 24l (Al5), 24l (Al6), 6f (Al7), 12j (Al8) and 12k (Al9) (Table S1). All the sites are fully occupied with the chemical formula $Al_{114}Fe_{24}$. The Si content was not determined using the X-ray diffraction method, and the Si atoms were assumed to be uniformly distributed at the Al sites [30].

To obtain detailed information about Si effects at the Al sites, we used two kinds of methods to replace Al atoms with Si. One method is using the configurations, with one

Si atom replacing one Al atom at each of the nine Al sites. These configurations lose their symmetry. The second method is a full replacement of Al atoms by Si at each Al site, keeping the system symmetry. The results are listed in Table 2.

Table 2. The calculated results (lattice parameters, coordination numbers of Si, and the formation energies via Equation (1) (ΔE_{f1}) and Equation (2) (ΔE_{Si}) for configurations with 1Si or full occupation at the Al sites. The bond lengths were chosen to be shorter than 3.0 Å. The unit of formation energies, ΔE_{f1}, is eV/Fe according to Equation (1), and ΔE_{Si} is eV/(cell) according to Equation (2), respectively. The values in bold italics indicate that the corresponding configurations are stable.

Si at Al Sites	Latt. Parameters (Å) and Vol. (Å^3/cell)				Local Coordination of Si by Fe/Mn	ΔE_{f1} (eV/Fe)/ΔE_{Si} (eV/(cell))
	a	*b*	*c;*	*V*		
$Al_{114}Fe_{24}$	12.622,	12.622,	12.622;	2011.06	-	−1.315/0
6Si at Al1	12.590,	12.590,	12.590;	1995.53	Si has two Fe and ten Al.	−1.169/+3.501
1Si1	12.595,	12.626,	12.623;	2007.45	Si1 has two Fe and ten Al.	~/+0.596
6Si at Al2	12.603,	12.603,	12.603;	2001.68	Si has two Fe, one Si, and 12 Al.	−1.133/+4.267
1Si2	12.600,	12.634,	12.629;	2010.32	Si2 has two Fe and 11 Al.	~/+0.697
12Si at Al3	12.570,	12.570,	12.570;	1986.08	Si has one Fe, five Si, and five Al.	−0.234/+3.469
1Si3	12.612,	12.619,	12.626;	2009.35	Si1 has one Fe and ten Al.	***~/−0.064***
12Si at Al4	12.553,	12.553,	12.553;	1978.30	Si has one Fe, five Si, and five Al.	−0.326/+1.260
1Si4	12.606,	12.612,	12.620;	2006.31	Si1 has one Fe and ten Al.	***~/−0.278***
24Si at Al5	12.635,	12.635,	12.635;	2017.15	Si has two Fe and nine Al.	−0.770/0.668
1Si5	12.620,	12.613,	12.619;	2008.57	Si has three Fe and nine Al.	~/+0.498
24Si at Al6	12.637,	12.637,	12.637;	2017.89	Si has two Fe and nine Al.	−0.770/+0.668
1Si6	12.626,	12.667,	12.621;	2018.55	Si has three Fe and nine Al.	~/+0.498
6Si at Al7	12.587,	12.587,	12.587;	1993.96	Si has two Fe and ten Al	−1.327/***−0.283***
1Si7	12.623,	12.636,	12.594;	2008.78	Si1 has two Fe and eight Al, with a long Fe-Al bond (~3.01 Å)	***~/−0.001***
12Si at Al8	12.547,	12.547,	12.547;	1975.02	Si has three Fe, one Si, and 7 Al.	−0.241/+0.275
1Si8	12.627,	12.610,	12.609;	2007.73	Si8 has three Fe and eight Al.	~/+0.257
12Si at Al9	12.567,	12.567,	12.567;	1984.85	Si has two Fe, one Si, and six Al	−0.122/0.514
1Si9	12.612,	12.617,	12.615;	2007.49	Si1 has two Fe and seven Al.	~/+0.487

The calculations revealed a wide variety of Si stabilization effects on the Al sites. There are three different types of consequences of Si doping at the Al sites (Table 2): high energy costs (ΔE_{Si} ~0.5 eV/Si) for one Si atom to replace one Al atom at the Al1, Al2, Al5, Al6 and Al9 sites; a moderate energy cost (0.26 eV/Si) for the Al8 site and the negative formation energies for one Si atom at the Al3 (−0.06 eV/Si), Al4 (−0.28 eV/Si) and Al7 (−0.001 eV/Si) sites. Interestingly, the formation energy of the system increases with increasing Si content and reaches a maximum when full occupation occurs at the Al7 sites. At the same time, a low Si occupation at both Al3 and Al4 sites has negative formation energies, whereas the formation energies become positive with high Si occupations. The relations between the formation energies and Si content at the Al3, Al4, and Al7 sites were shown in Figure 1a, with the formation energies being obtained according to Equation (3) with the unit meV/Fe.

The formation energy (ΔE_{Si}) decreases as the Si content increases at the Al7 sites and reaches a minimum at full occupation (ΔE_{Si} = −0.28 eV/cell) (Table 2). It decreases with Si content up to about one-quarter occupation at the Al3 sites, with formation energy, $\Delta E_{Si,}$ being −0.15 eV/cell. It is notable that Si occupation at five of the twelve Al4 sites has the lowest formation energy, ΔE_{Si} = −0.95 eV/cell or −40 meV/Fe in Figure 1a.

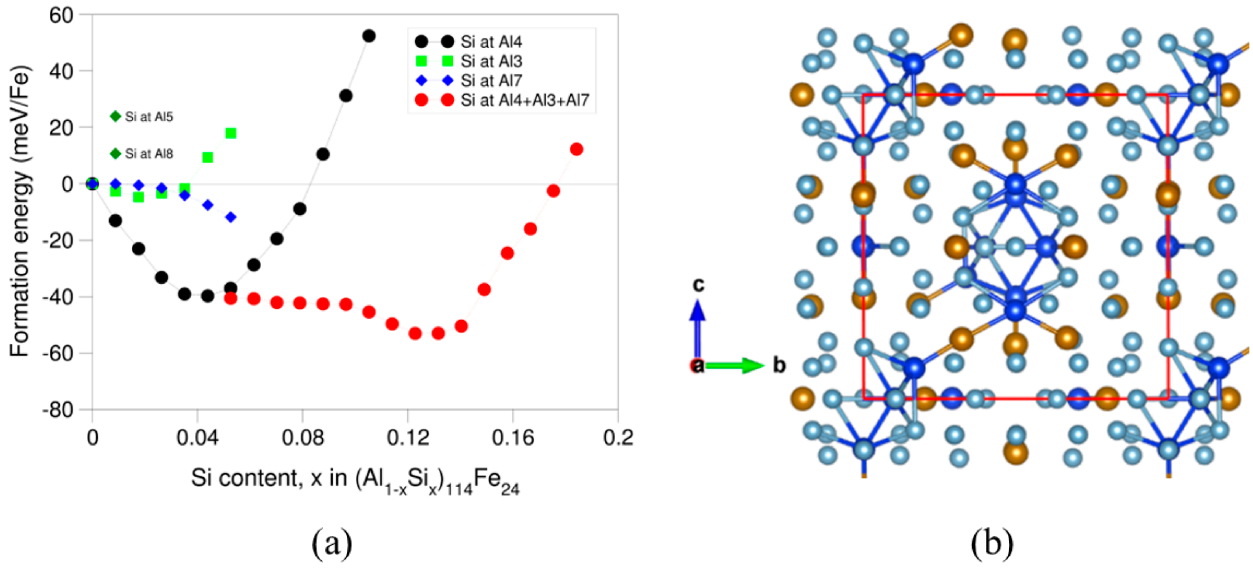

Figure 1. (**a**) The calculated relationship between the formation energy and the Si content for the highly stable configurations of the cubic α-$(Al_{1-x}Si_x)_{114}Fe_{24}$ (ΔE_{Si2}) according to Equation (3) and (**b**) the schematic structure of α-$(Al_{0.8772}Si_{0.1228})_{114}Fe_{24}$. The red square in (**b**) represents the *b*- and *c*-axis.

The above-mentioned results helped design Si doping at the Al sites. The evolution of Si in the cubic α-$Al_{114}Fe_{24}$ with high stability starts from Si replacements at the Al4 sites to 5/12 occupation with its minimum energy, then Si atoms are added to Al3 sites, and then to the Al7 sites. The relation between the formation energy and the Si content at the mixed Al4, Al3, and Al7 sites is shown in Figure 1a. The most stable configuration has a full Si occupation at the Al7 sites and a partial occupation at the Al3 and Al4 sites, and in total, 14 Si atoms in the cell, or x(Si) = 0.1228 with $\Delta E_{Si} = -1.275$ eV/cell (or −53 meV/Fe in Figure 1a). Figure 1 reveals a shallow potential well between x = 0.10 and 0.15 in α-$(Al_{1-x}Si_x)_{114}Fe_{24}$ or α-$(Al_{1-x}Si_x)_{4.75}Fe$, which indicates the flexibility of the chemical composition range. A schematic structure of α-$(Al_{0.8772}Si_{0.1228})_{4.75}Fe$ is shown in Figure 1b. This model provided the Si distribution at the specific Al sites and updated the experimental model [30].

The partial occupation of Si at the Al3 and Al4 sites means extra freedom in the cubic α-$(Al_{1-x}Si_x)_{4.75}Fe$ phase. Furthermore, the rather shallow potential well indicates the flexibility of this structure. Therefore, one expects a broad range of Si contents in the samples prepared or manufactured at high temperatures, typically over 1000 K, depending on the local chemical environment.

3.3. Si Stabilizing the Hexagonal α'-AlFe Phase

The crystal structure of the hexagonal α'-AlFeSi phase has been investigated intensively [31,32,58,59]. Corby and Black [31] in 1977 reported the detailed structure of α'-AlFeSi based on the anomalous-dispersion methods from the single-crystal X-ray diffraction pattern. Its lattice was determined to be hexagonal with space group $P6_3/mmc$ (Nr. 194). The structure exhibits a complex nature with 23 crystallographically different atomic sites: five Fe sites and eighteen Al sites. Among the five Fe sites, three are at 12k sites (Fe1, Fe2, Fe3), one is at 6h (Fe4), and one is at 4f (Fe5). All the iron sites are fully occupied within the errors of the measurements. Among the eighteen Al sites, fifteen of them are almost fully occupied, and three of them are partially occupied (Table S1). Recently, Roger et al. revisited this phase using a single-crystal X-ray diffraction approach with the chemical formula $Al_{7.1}SiFe_2$ [32]. They also identified the Si sites: Si1 at 12k (Al4 sites according to our note), Si2 at 6h (Al17 sites here), and Si3 at 2c (Al18 sites here). Both Si2 and Si3 are mixed with

Al atoms: Si2 (Al17) has a mixture of atoms with a large Si occupation of 0.85 and a small Al occupation of 0.15 (Al17). Meanwhile, Si3 (Al18) has a moderate occupation of 0.14 [32]. The experimental result provided the starting point for investigating the Si stabilization effect in the hexagonal α′-AlFe phase.

The calculated formations for the configurations of the binary α′-AlFe phase are shown in Table 1. We chose Config-2 in Table 1 to investigate the Si stabilization effect in this phase, considering the low occupation rate of Al(Si) at the Al18 or Si3 sites [31,32]. The calculated relationship between the formation energy and Si content according to Equation (3) is shown in Figure 2a.

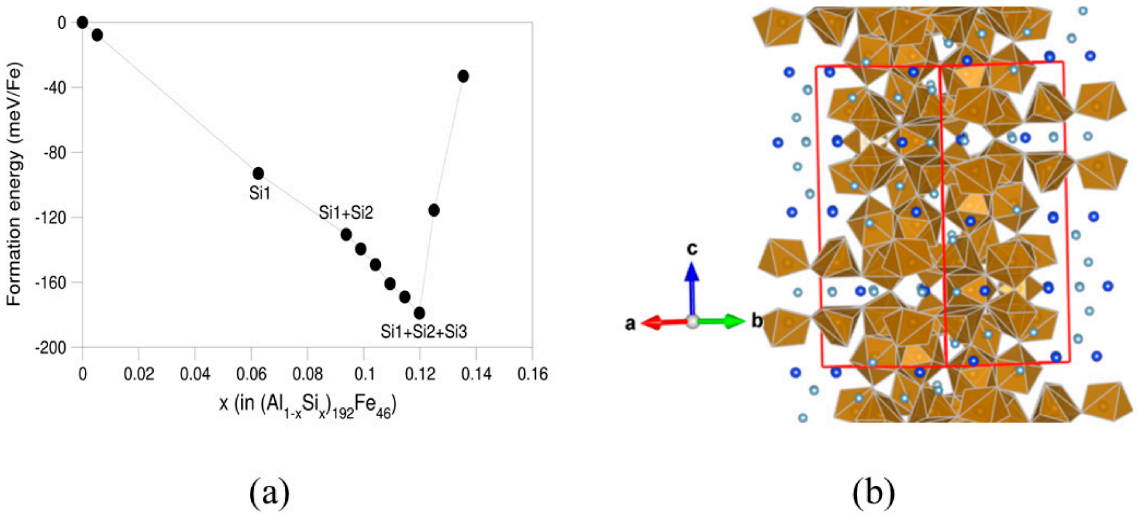

Figure 2. (**a**) The calculated relation between the formation energy and Si content for the highly stable configurations of α′-$(Al_{1-x}Si_x)_{192}Fe_{46}$ (ΔE_{Si2}) according to Equation (3). (**b**) The schematic structure for the most stable configuration with x = 0.1198. The dotted line in (**a**) is to guide readers' eyes. The red lines in (**b**) illustrate the unit cell with the axis shown on the left.

The Si atoms were first added to the Al4 sites, which is Si1 in [32]. The configuration with one Si atom at Al4 has a moderate negative formation energy (−0.47 eV/cell or −0.01 eV/Fe). The full Si occupation of the Al4 sites (x(Si1) = 0.0625) caused a formation energy of −93 meV/Fe as shown in Figure 2a. Then six Si atoms were used to replace the Al14 sites (Si2 sites) (x(Si1 + Si2) = 0.09375), and the formation energy became −131 meV/Fe. Further doping Si at the 6h (Al17) or Si3 sites in [32] reduces the formation energy until five of the Al atoms are replaced with x(Si) = 0.1198, and the formation energy is calculated to be −179 meV/Fe. Interestingly, adding another Si at the Al17 sites to have a full occupation at the sites raises the formation energy to −116 meV/Fe. Thus, the present calculations provided x(Si) = 0.1198 in $(Al_{1-x}Si_x)_{192}Fe_{46}$ is slightly less than x(Si) = 0.1235 in the formula $Al_{7.1}SiFe_2$ [32]. The slightly higher Si content in the experiment may originate from the partial occupation of the 2c (Al18 [31] or Si3 [32]) sites and kinetic factors at the formation temperature. Meanwhile, our calculations provided a Si occupation of 5/6 at the Al17 sites, which is in good agreement with the experimental observation of a Si occupation of 0.85 [32].

Overall, the present ab initio study produced a rather sharp potential well for the Si solution at the specific Al sites (full replacement at the Al4, Al14, and partial replacement at Al17). The most stable structure has the chemical formula $(Al_{0.8802}Si_{0.1198})_{192}Fe_{46}$ or $(Al_{0.8802}Si_{0.1198})_{4.174}Fe$. This study has confirmed the experimental results with consideration of the extra freedom for the Si in the experimental results [32]. The calculations revealed a notably significant Si stabilization effect on the hexagonal phase with ΔE_{Si2} = −179 meV/Fe compared with that in the cubic phase (−53 meV/Fe).

3.4. Si Stabilization Effects on the Al-Rich Binary Fe-IMCs

In the Al-rich part of the binary Al-Fe phase diagram [2,36,60], there is a series of Fe-IMCs. Wolverton and Ozolins [36] investigated several Fe-IMCs, including (θ-)$Al_{13}Fe_4$ and (η-)Al_6Fe with the Al_6Mn-type structure. In recent years, the frequently observed Al-rich binary and the related ternary Fe-IMCs, including η-Al_6Fe [44], τ_4-$(Al,Si)_5Fe$ [46], β-$Al_{4.5}SiFe$ [45], and θ-$(Al,Si)_{13}Fe_4$ [47,48] were investigated. Here, we revisited these compounds together with the above-mentioned cubic α- and hexagonal α'-AlFe(Si) phases in a systematic way. A novel phase, $Al_{12}Fe$, which is assumed to have the $Al_{12}Mn$-type structure [61], was also investigated. The obtained relations between the formation energies and the Fe contents for the binary and ternary Fe-IMCs are plotted in Figure 3. The results (calculated lattice parameters and formation energies) of these Fe-IMCs are listed in Table 3.

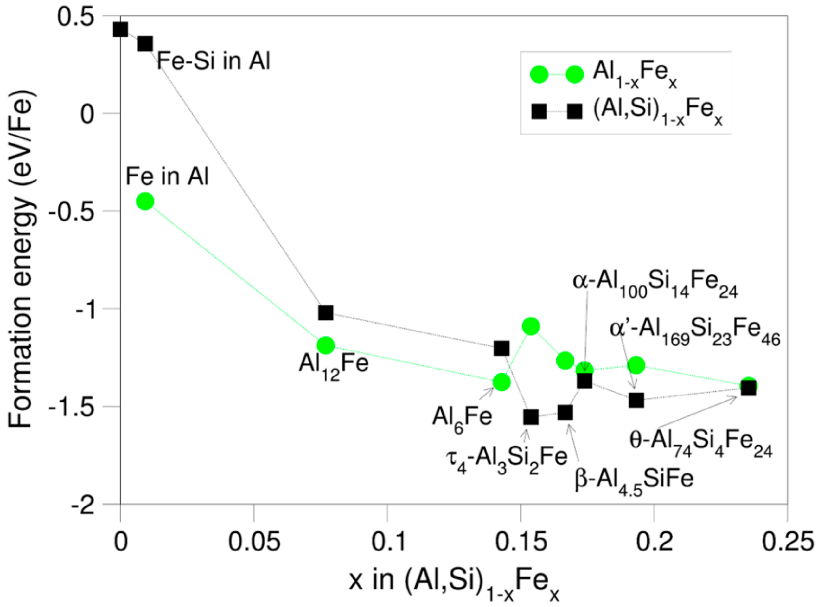

Figure 3. Summary of the comparison of the calculated formation energies (ΔE_f) for the Al-rich binary AlFe (green spheres) and ternary AlFeSi compounds (black squares) with respect to the elemental solids, α-Al, Si and α-Fe according to Equation 1. The dotted lines are used to guide reader's eyes.

The calculations showed that a diluted solution of an iron atom in the Al matrix gains energy with the formation energy ($\Delta E_f = -0.45$ eV/Fe, Table 1). Meanwhile, a solution of a Si atom in the Al matrix costs energy ($\Delta E_f = +0.43$ eV/Si). The calculations also revealed that the formation of a Si-Fe pair in the Al matrix costs about 0.36 eV (Fe-Si), being lower than that of pure Si solution. As shown in Table 3, the calculated formation energies of the Al-rich Fe-IMCs are very close to the previous first-principles DFT calculations [44–48,62].

The present investigation on the stability and the Si stabilization effects on α'- vs. α- represents the fact that Si changes the ordering in solidification on the chemical environments. As shown in Figure 3, the relative stability of the binary Fe-IMCs (from high stability (with low formation energy) to low stability (with high formation energy)) has the following series:

$$\theta\text{-}Al_{13}Fe_4 > \eta\text{-}Al_6Fe > \alpha\text{-} > \alpha'\text{-} > \tau_4\text{-}Al_{5.5}Fe > Al_{12}Fe > \beta\text{-}Al_{5.5}Fe\ (> \text{Fe solution in Al}) \quad (4)$$

The top three stable binary compounds are θ-$Al_{13}Fe_4$, η-Al_6Fe, and the cubic α-AlFe. This agrees with thermodynamics study on the Al-Fe binary phase diagram that θ-$Al_{13}Fe_4$ is the only stable phase in the Al-rich region (x(Fe) < 24.0 at%) [22,60]. Moreover, the

experimental observations revealed that cubic α-AlFe (in Chinese Script [1,3,49]), θ- and η-Al_6Fe particles are frequently observed in Si-poor conditions [1–4,63].

Table 3. The calculated lattice parameters and formation energies with references to the elemental solids via Equation (1) for the frequently observed binary Fe-IMCs and the related ternary Fe-IMCs. Experimental data from the literature were included for comparison. The optimized lattice parameters for $\alpha(Al_{0.8772}Si_{0.1228})_{4.75}Fe$, α'-$(Al_{0.8802}Si_{0.1198})_{4.174}Fe$, and $\theta(Al_{0.949}Si_{0.051})_{13}Fe_4$ with broken symmetry are the averaged values, as they differ moderately from the ones with symmetry.

Binary, Fe-IMCs				**Ternary Fe-IMCs**			
Phase	Latt. S.G.	Paras. (Å)	ΔE_f (eV/Fe)	Phase	Latt.S.G.	Paras.(Å)	ΔE_f (eV/Fe)
$Al_{12}Fe$	Cubic Im-3 (204)	a = 7.464	−1.19	-	-	-	-
η-Al_6Fe	Orth. Cmcm (63)	a = 6.465 (6.492) [24] b = 7.420 (7.437) c = 8.795 (8.788)	−1.38 −1.38 [44] −1.35 [62]	-	-	-	-
τ_4-Al_5Fe	Tetr. I4/mcm (140)	1 = 6.262 (-) b = 6.262 (-) c = 9.625 (-)	−1.09 −1.09 [46]	τ_4-Al_3Si_2Fe	Orth. Pbcn(60)	a = 6.057 (6.061) [26] b = 6.061 (6.061) c = 9.483 (9.525)	−1.554 −1.55 [46]
β-$Al_{5.5}Fe$	Monic. A2/a (15)	a = 6.240 (-) b = 6.240 (-) c = 21.087 (-) β = 90.34° (-)	−1.27 −1.27 [45]	β-$Al_{4.5}SiFe$	Monic. A2/a(15)	a = 6.165 (6.161) [28] b = 6.165 (6.175) c = 20.766 (20.813) β = 91.43° (90.42°)	−1.531 −1.53 [45]
α-$Al_{4.75}Fe$	Cubic Pm-3 (200)	a = 12.622 (12.56) [30]	−1.32	α $(Al_{0.8772}Si_{0.1228})_{4.75}Fe$	Tricl. P-1(2)	a = 12.534 (12.56) [30]	−1.369
α'$Al_{4.174}Fe$	Hex. $P6_3/mmc$ (194)	a = 12.447 (-) c = 26.370 (-)	−1.29	α' $(Al_{0.8802}Si_{0.1198})_{4.174}Fe$	Tricl. P-1 (2)	a = 12.347 (12.345) [32] c = 26.222 (26.210)	−1.468
θ-$Al_{13}Fe_4$	Monoc. C2/m (12)	a = 15.426 (15.492) [33] b = 8.022 (8.078) c = 12.425 (12.471) β = 107.68° (107.69°)	−1.401 −1.40 [48] −1.40 [62]	$\theta(Al_{0.949}Si_{0.051})_{13}Fe_4$	Tricl. P-1(2)	a = 15.380 (15.492) [33] b = 8.012 (8.078) c = 12.343 (12.471) β = 107.62° (107.69°)	−1.406 −1.41 [48]

This study revealed that the Si solution in these compounds has different effects on their stability. For the binary Fe-IMCs with low Fe contents, novel $Al_{12}Fe$, and η-Al_6Fe, the Si solution at the Al sites costs energy. The calculations also revealed strong Si stabilization effects on the τ_4- and β-phase and moderate Si stabilization effects on the α- and θ-phase. It is noted that the Si solution stabilized the hexagonal α'-phase much more than the α-phase. The results cause a change in the stability series of the ternary Fe-IMCs as compared with the binary ones. For the Al-rich ternary Fe-IMCs, the stability series is,

$$\tau_4\text{-}(Al,Si)_5Fe > \beta\text{-}Al_{4.5}SiFe > \alpha' > \theta > \alpha\text{-phase} (> > \eta\text{-}Al_6Fe > Al_{12}Fe) \quad (5)$$

The top three compounds of high stability in the Al-Fe-Si system are τ_4-$(Al,Si)_5Fe$, β-$Al_{4.5}SiFe$, and the hexagonal α'-phase, which differs notably from that in the binary series (Equation (4)). The notably different stability series in Equations 4 and 5 is reflected in the formation of the Fe-IMCs during the casting of Al metals with different contents of Si.

4. Discussion

The present calculations revealed the stability of the binary Fe-IMCs at 0 K in Equation (3). The most stable three Fe-IMCs are θ-$Al_{13}Fe_4$ > η-Al_6Fe >α-$Al_{4.75}Fe$, indicating the formation predominance of these compounds during casting in Si-poor Al metals. The predicted results in Equation (3) agree with the experimental observations [1–3,19,49,63,64] that θ-$Al_{13}Fe_4$, η-Al_6Fe with some Mn/Fe mixture, and α-$Al_{4.75}Fe$ particles are formed and observed as primary intermetallic compounds in Si-poor conditions. Meanwhile, in

Si-rich Al alloys, the Fe-IMCs with the highest stability are τ_4-$(Al,Si)_5Fe$ > β-$Al_{4.5}SiFe$ > α′-phase, which agrees with the experimental observations. It is noted that the present study about the stability of the Fe-IMCs provides idealized structural models at T = 0 K and p = 0 Pa. Other factors, such as impurity, lattice vibration, and electron excitation contributions to the stability of the compounds at elevated temperatures, were not taken into account. The obtained information may help readers understand the physics behind the experimental observations.

The present work provides an opportunity to discuss the impacts of Si content on the formation of Fe-IMCs during the solidification and thermal treatment of Al alloys. Here, we first address the Si influences on the α- and α′-phases as examples.

As shown in Table 3, the content of Si solution in the cubic α-AlFe phase (x ≈ 0.122 in $(Al_{1-x}Si_x)_{4.75}Fe$) is close to that in the hexagonal α′-phase (x ≈ 0.120 in α′-$(Al_{1-x}Si_x)_{4.174}Fe$). Moreover, there are partial Si occupations at some Al sites, which means that the system symmetry has been broken in both crystals (Table 3). A careful analysis of the ab initio investigations produced the following diverse results:

(i). Si stabilization effect varies with a moderate effect on cubic α-phase ($\Delta E_{Si2} = -0.054$ eV/Fe) and a strong impact on the hexagonal α-phase ($\Delta E_{Si2} = -0.181$ eV/Fe).

(ii). The compositional flexibility is different in the two phases: a shallow potential valley between x = 0.10 to 0.15 for the cubic α-$(Al_{1-x}Si_x)_{4.75}Fe$ crystal, indicating high flexibility of the chemical composition. Whereas there is a sharp energy well in the energy/Si content relation, indicating the rigidity of its chemical composition for the α′-phase.

(iii). There are different degrees of extra freedoms caused by the Si partial occupation at the specific Al sites in the two phases. For the cubic α-$(Al_{1-x}Si_x)_{4.75}Fe$ phase, the most stable configuration contains partial occupation of Al3 (12j) and Al4 (12j) sites (eight Si at the 24 Al positions, see Section 3B), representing the number of independent configurations, $w = [(12 \times 11 \times 10 \times 9)/(4 \times 3 \times 2 \times 1)] \times [(12 \times 11 \times 10 \times 9)/(4 \times 3 \times 2 \times 1)] = 245{,}024$. This indicates configurational entropy contributions, $S_{conf} = R \ln w = 8.617 \times 10^{-5}$ (eV/K) $\times 12.409 = 1.07 \times 10^{-3}$ (eV/K) per cell and TS_{conf} = 1.07 eV/cell or 0.045 eV/Fe at 1000 K. Meanwhile, in α′-$(Al_{1-x}Si_x)_{4.174}Fe$, only Si at Al17 (6h sites) has occupation (5/6), which gives w = 6 and consequently $S_{conf} = R \ln w = 8.617 \times 10^{-5}$ (eV/K) $\times 1.792 = 0.154 \times 10^{-3}$ (eV/K) per cell and TS_{conf} = 0.154 eV/cell or 0.003 eV/Fe at 1000 K.

Overall, according to the Gibbs law, $\Delta G = \Delta H - T\,\Delta S = -1.369 - 0.045 = -1.414$ eV/Fe for the cubic phase and $\Delta G = \Delta H - T\,\Delta S = -1.468 - 0.003 = -1.471$ eV/Fe for the hexagonal phase at 1000 K, respectively. These estimations suggested that under the casting conditions, the hexagonal phase is still more stable than the cubic phase in high Si alloys.

Table 3 showed that the Si stabilization effect on the binary Fe-IMCs relates to the Si content in the ternary ones. The related formation energy differences due to Si addition according to Equation (3) are shown in Figure 4.

Figure 4 shows that the formation energies, due to Si joining at the Al sites, decrease with increasing Si content. This relation between the formation of Fe-IMCs and the Si contents helps us to understand the formation mechanisms of Fe-IMCs during solidification and the thermal treatments of Al alloys with different Si contents.

The formation of Fe-IMCs during casting is a complex process, and it depends on the thermodynamics and kinetic factors, as well as the compositional and structural templates used [2–4,19,49,63,64]. The present study provided thermal properties, including formation energies (enthalpies) and configurational contributions of the Fe-IMCs. Meanwhile, other kinetic factors, such as temperature and cooling rates, as well as local impurities and their compositions due to inhomogeneity and local structures, also play crucial roles in the formation of Fe-IMCs.

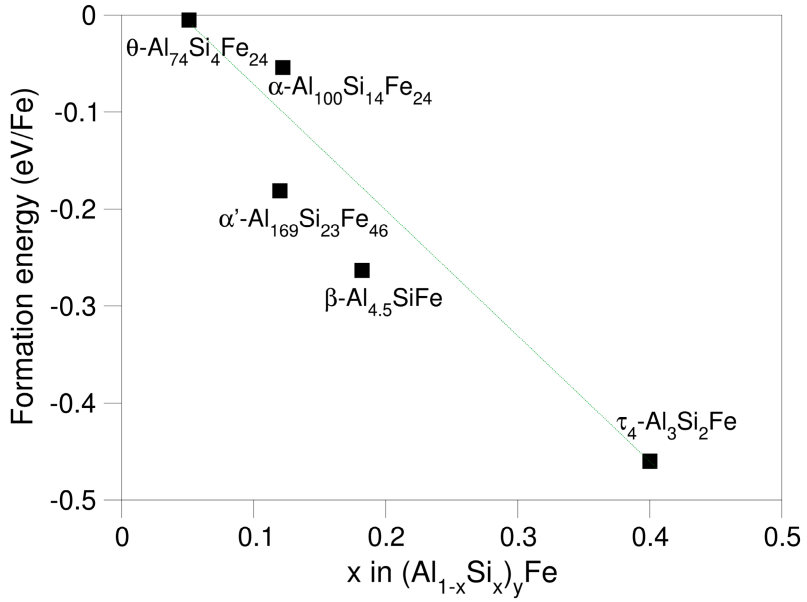

Figure 4. Dependence of formation energy, ΔE_{Si2}, on the Si content in the ternary Fe-IMCs according to Equation (3). The dotted dark-green line is used to illustrate a linear relation.

In practice, Al metals/alloys, particularly those from scraps and waste, contain more impurities, including other 3D and 4D/5D transition metals beyond the well-known Fe and Si. These transition metal elements may replace Fe to form multiple transition metal alloys with huge numbers of extra freedoms (high-entropy contributions), which may change not only the formation of the Fe-IMCs but also the co-joining Si [14,19,40,42,44,65]. This topic deserves comprehensive investigations, particularly the competencies among the Fe-IMCs phases.

Moreover, vacancy distribution in the Fe-IMCs might be very complex and may contain long-distance distributions, particularly at elevated temperatures. In this study, we only used the conventional cells of the cubic α- and the hexagonal α-phases due to the limitation of the electronic DFT approaches [34,54]. Meanwhile, the relatively large unit cells (axis lengths are larger than 12 Å) indicate that the present parameter-free quantum mechanics-based approach provided the essence of the vacancy formation, which can be used for further modeling using other approaches, e.g., cluster expansion [66].

The systematic knowledge in this study helps us to understand the formation of the Fe-IMCs in Al-based alloys with different chemical compositions and design novel Al-based alloys of desirable mechanical and chemical properties from, for example, Al scraps/wasters by means of chemical approaches [67,68]. Furthermore, this knowledge could be applied to new tools like AI and machine learning [69,70].

5. Conclusions

The Si stabilization effects on the binary cubic α- and ternary α'-AlFe phases were investigated using the first-principles DFT method. The study revealed that the addition of Si changed the relative stability of the two phases and that Si strongly stabilizes the hexagonal α'-phase and moderately stabilizes the cubic α-phase. Consequently, the cubic α-particles are more likely to form in Si-poor conditions, while the hexagonal phase forms in Si-rich Al alloys.

A systematic study on the frequently observed Fe-IMCs revealed that for Si-poor Al alloys, the order series of stability is θ-$Al_{13}Fe_4$ > η-Al_6Fe >α-$Al_{4.75}Fe$ (Equation (4)). The addition of Si changed this series. For Si-rich Al metals, the order series of stability becomes τ_4-$(Al,Si)_5Fe$ > β-$Al_{4.5}SiFe$ >α'-$(Al,Si)_{4.174}Fe$ (Equation (5)). The obtained information here

not only helps us to understand the formation of Fe-IMCs in Al casting and thermal treatment but also to design new casting conditions and new Al alloys of desirable properties from, for example, Al scraps/wastes.

Supplementary Materials: The following supporting information can be downloaded at https://www.mdpi.com/article/10.3390/met16080832/s1. Table S1. Atomic coordinates and local symmetry of atomic species in the cubic α-(AlFeSi) phase (Model 3) by Cooper [30]. The space group is Pm-3 (No. 200) with a = 12.56 Å [30]. All the atomic sites were fully occupied with occupation rate to be 1.0. Note that the original Al8, Al10 and Al12 are unoccupied and thus, *the original Al9 becomes Al8 and original Al11 becomes Al9 here. The chemical formula is α-$Al_{114}Fe_{24}$. Table S2. Atomic coordinates and occupation at the Wyckoff sites from the experimental models for the hexagonal α′-(AlFeSi) phase by Corby and Black [31], (left). The space group is $P6_3/mmc$ (194) with a = 12.404 Å and c = 26.234 Å [31] and that by Roger et al. with a = 12.3445 Å and c = 26.210 Å [32] (right). There are Mn atoms at the Fe sites and the Si atoms distribute homogeneously at the Al sites in [31]. The fractional atomic coordinates in right were changed according to the symmetry operations in the space group in [31] for comparison.

Author Contributions: Conceptualization, C.F.; Methodology, C.F.; Software, C.F.; Validation, C.F.; Formal analysis, C.F.; Investigation, C.F.; Resources, C.F.; Data curation, C.F.; Writing—original draft, C.F.; Writing—review and editing, C.F., Z.Q., and Z.F.; Visualization, C.F.; Supervision, Z.F.; Project administration, C.F. and Z.Q.; Funding acquisition, Z.F. All authors have read and agreed to the published version of the manuscript.

Funding: This research was funded by the Engineering and Physical Sciences Research Council (EPSRC, UK), grant numbers EP/v011804/1 and EP/S005102/1.

Data Availability Statement: The original contributions presented in this study are included in the article/supplementary material. Further inquiries can be directed to the corresponding author.

Conflicts of Interest: The authors declare no conflicts of interest.

References

1. Mondolfo, L.F. *Aluminum Alloys: Structure and Properties*; Butterworths: London, UK, 1976.
2. Khalifa, W.; Samuel, F.H.; Gruzleski, J.E. Iron intermetallic phases in the Al corner of the Al-Si-Fe system. *Metal. Mater. Trans. A* **2003**, *34*, 807–825. [CrossRef]
3. Zhang, H. Effect of iron on the microstructure and mechanical properties of Al-Si alloys. *Miner. Met. Mater. Soc.* **2007**, 775–780.
4. Glazoff, M.L.; Khvan, A.; Zolotorevsky, V.S.; Belov, N.A.; Dinsdale, A. *Casting Aluminum Alloys: Their Physical and Mechanical Metallurgy*; Butterworth-Heinemann: Oxford, UK, 2018.
5. Schlesinger, M.E. *Aluminum Recycling*; CRC Press: Boca Raton, FL, USA, 2006.
6. Reuter, M.A.; van Schaik, A.; Gutzmer, J.; Bartie, N.; Abadías-Liamas, A. Challenges of the circular economy: A material, Metallurgical, and Product design perspective. *Ann. Rev. Mater. Res.* **2019**, *49*, 253–274. [CrossRef]
7. Kotadia, H.R.; Bareker, N.; Khan, M.H.; Ahuir-Torres, J.L.; Das, A. Aluminium recycling: A critical review of iron-bearing intermetallics in alloys. *Mater. Today Sustain.* **2025**, *30*, 101119. [CrossRef]
8. Chen, H.B.; Xie, Y.L.; Tang, P.; Tang, Z.Y.; Liao, C.W.; Pang, R.H. Demystifying the influence of scrap to raw material ratio on the microstructural and mechanical properties of the secondary 7075 aluminum alloy. *Mater. Lett.* **2025**, *382*, 137847. [CrossRef]
9. Zhang, Y.K.; Lei, Y.; Ren, Y.S.; Ma, W.H. Removal of Fe impurities from Al alloy scraps by electromagnetic directional solidification combined with Si addition. *J. Mater. Res. Techn.* **2023**, *26*, 8738–8747. [CrossRef]
10. Gaustad, G.; Olivetti, E.; Kirchain, R. Improving aluminum recycling: A survey of sorting and impurity removal technologies. *Resour. Conserv. Recycl.* **2012**, *58*, 79–87. [CrossRef]
11. Liddicoat, P.V.; Liao, X.-Z.; Zhao, Y.H.; Zhu, Y.T.; Murashkin, M.Y.; Lavernia, E.J.; Valiev, R.Z.; Ringer, S.P. Nanostructural hierarchy increases the strength of aluminium alloys. *Nat. Commun.* **2010**, *1*, 63. [CrossRef] [PubMed]
12. Qin, L.M.; Tang, P.; Meng, S.X. Effect of Ni addition on the microstructure, conductivities and mechanical properties of as-cast Al-Fe alloys. *J. Alloys Compd.* **2024**, *986*, 174160. [CrossRef]
13. Warmuzek, M. Chemical composition of the Ni-containing intermetallic phases in the multicomponent Al alloys. *J. Alloys Compd.* **2014**, *604*, 245–252. [CrossRef]

14. Cai, Q.; Fang, C.M.; Lordan, E.; Wang, Y.; Chang, I.T.H.; Cantor, B. A novel Al-Si-Ni-Fe near-eutectic alloy for applications at elevated temperatures. *Scr. Mater.* **2023**, *237*, 115707. [CrossRef]
15. Chen, S.L. Recycling of Metals: Importance, Processes, and Future Directions. *J. Powder Metall. Min.* **2024**, *13*, 1000441.
16. Raabe, D.; Tasan, C.C.; Olivetti, E.A. Strategies for improving the sustainability of structural metals. *Nature* **2019**, *575*, 64–74. [CrossRef] [PubMed]
17. Zhu, Y.; Cooper, D.R. An optimal reverse material supply chain for US aluminum scrap. *Procedia CIRP* **2019**, *80*, 677–682. [CrossRef]
18. Park, S.-W.; Kayani, S.H.; Park, J.-W.; Lee, M.-Y.; Kim, J.H. Mitigating Fe-rich intermetallic embrittlement in Al-Si-Cu-Mg alloys by deformation-assisted semi-solid rolling. *J. Alloys Compd.* **2026**, *1065*, 188238. [CrossRef]
19. Que, Z.P.; Wang, Y.; Fan, Z. Formation of the Fe-containing intermetallic compounds during solidification of Al-5Mg-2Si-0.7Mn-1.1Fe alloy. *Metal. Mater. Trans. A* **2018**, *49*, 2173–2181. [CrossRef]
20. Taylor, J. Iron-Containing Intermetallic Phases in Al-Si Based Casting Alloys. *Procedia Mater. Sci.* **2012**, *1*, 19–33. [CrossRef]
21. Zienert, T.; Leineeber, A.; Fabrichnaya, O. Heat capacity of Fe-Al intermetallics: B2-FeAl, $FeAl_2$, Fe_2Al_5 and Fe_4Al_{13}. *J. Alloys Compd.* **2017**, *725*, 848–859. [CrossRef]
22. Sundman, B.; Ohnuma, I.; Dupin, N.; Kattner, U.R.; Fries, S.G. An assessment of the entire Al-Fe system including $D0_3$ ordering. *Acta Mater.* **2009**, *57*, 2896–2908. [CrossRef]
23. Marker, M.C.J.; Skolyszewska-Kühberger, B.; Effenberger, H.S.; Schmetterer, C.; Richter, K.W. Phase equilibria and structural investigations in the system Al-Fe-Si. *Intermetallics* **2011**, *19*, 1919–1929. [CrossRef] [PubMed]
24. Walford, L.K. The structure of the intermetallic phase $FeAl_6$. *Acta Cryst.* **1965**, *18*, 287–291. [CrossRef]
25. Pandy, P.K.; Schubert, K. Strukturuntersuchungen in einigen mischungen T-B3-B4 (T = Mn, Fe, Co, Ir, Ni, Pd; B3 = Al, Ga, Tl; B4 = Si, Ge). *J. Less-Common Met.* **1969**, *18*, 175–202.
26. Gueneau, C.; Servant, C.; D'Yvoir, F.; Rodier, N. $FeAl_3Si_2$. *Acta Crystallogr. C* **1995**, *51*, 177–179. [CrossRef]
27. Carpenter, G.J.; Lepage, Y. Revised cell data for the β-FeSiAl phase in aluminum alloys. *Scr. Metall. Mater.* **1993**, *28*, 733–736. [CrossRef]
28. Rømming, C.; Hansen, V.; Gjønnes, J. Crystal structure of β-$Al_{4.5}$FeSi. *Acta Crystallogr. B* **1994**, *50*, 307–312. [CrossRef]
29. Hansen, V.; Hauback, B.; Sundberg, M.; Rømming, C.; Gjønnes, J. B-$Al_{4.5}$FeSi, A combined synchrotron powder diffraction, electron diffraction, high-resolution electron microscopy and single-crystal X-ray diffraction study of a faulted structure. *Acta Crystallogr. B* **1998**, *54*, 351–357. [CrossRef]
30. Cooper, M. The crystal structure of the ternary alloy α(AlFeSi). *Acta Cryst.* **1967**, *23*, 1106–1107. [CrossRef]
31. Corby, R.N.; Black, P.J. The structure of α-(AlFeSi) by anomalous-dispersion methods. *Acta Cryst. B* **1977**, *33*, 3468–3475. [CrossRef]
32. Roger, J.; Bosselet, F.; Viala, J.C. X-ray structural analysis and thermal stability studied of the ternary compound α-AlFeSi. *J. Solid State Chem.* **2011**, *184*, 1120–1128. [CrossRef]
33. Grin, J.; Burkhard, U.; Ellner, M.; Peters, K. Refinement of the Fe_4Al_{13} structure and its relationship to the quasihomogical homeotypical structures. *Z. Krist.* **1994**, *209*, 479–487.
34. Jones, R.J. Density functional theory: Its origins, rise to prominence, and future. *Rev. Mod. Phys.* **2015**, *87*, 897–923. [CrossRef]
35. Huang, B.; von Rudorff, G.F.; von Lilienfeld, G.F. The central role of density functional theory in the AI age. *Science* **2023**, *381*, 170–173. [CrossRef] [PubMed]
36. Wolverton, C.; Ozolinč, V. First-principles aluminum database: Energetics of binary Al alloys and compounds. *Phys. Rev. B* **2006**, *73*, 114104. [CrossRef]
37. Liu, Y.H.; Chong, X.Y.; Jiang, Y.H.; Zhou, R.; Feng, J. Mechanical properties and electronic structures of Fe-Al intermetallic. *Phys. B* **2017**, *506*, 1–11. [CrossRef]
38. Lafaye, P.; Duc Vo, M.; Jofre, J.; Harvey, J.-P. Investigating the Al/Si mixed site occupation in the β-AlFeSi phase. *Phys. Chem. Chem. Phys.* **2023**, *25*, 20015–20025. [CrossRef] [PubMed]
39. Becker, H.; Bulut, N.; Kortus, J.; Leineweber, A. B-Al4.5FeSi: Hierarchical crystal and defect structure: Reconciling experimental and theoretical evidence including the influence of Al vs. Si ordering on the crystal structure. *J. Alloys Compd.* **2022**, *911*, 165015. [CrossRef]
40. Popčevič, P.; Smontara, A.; Ivkov, J.; Wencka, M.; Komelj, M.; Jeglič, P.; Vrtnik, S.; Bohnar, M.; Jagliič, Z.; Baer, B.; et al. Anisotropic physical properties of the Al13Fe4 complex intermetallic and its ternary derivative $Al_{13}(Fe,Ni)_4$. *Phys. Rev. B* **2010**, *81*, 184203.
41. Ma, D.C. Elastic properties of Mn-rich α intermetallic phase in engineering aluminum alloy: An ab initio study. *J. Appl. Phys.* **2018**, *124*, 085109. [CrossRef]
42. Zhang, X.Z.; Wang, D.T.; Nagaumi, H.; Zhou, Y.X.; Yu, W.; Chong, X.Y.; Li, X.Z.; Zhang, H.T. Morphology, thermal stability, electron structure and mechanical properties of α-AlFeMnSi phases with varying Mn/Fe atomic ratios: Experimental studies and DFT calculations. *J. Alloys Compd.* **2022**, *25*, 163523. [CrossRef]
43. Amirkhanyan, L.; Weissbach, T.; Gruber, T.; Zienert, T.; Fabrichnaya, O.; Kortus, J. Thermodynamic investigation of the τ4-Al-Fe-Si intermetallic ternary phase: A density-functional theory study. *J. Alloys Compd.* **2014**, *598*, 137–141. [CrossRef]

44. Dinsdale, A.; Fang, C.M.; Que, Z.P.; Fan, Z. Understanding the thermodynamics and crystal structure of complex Fe containing intermetallic phases formed on solidification of Aluminium alloys. *JOM* **2019**, *71*, 1731–1736. [CrossRef]
45. Fang, C.M.; Que, Z.P.; Fan, Z. Crystal Chemistry and Electronic Structure of the β-AlFeSi phase from First-Principles. *J. Solid State Chem.* **2021**, *299*, 122199. [CrossRef]
46. Fang, C.M.; Que, Z.P.; Fan, Z. Stability, chemical composition, and structural and electronic properties of the intermetallic compound τ4-(Al,Si)5Fe. *J. Alloys Compd.* **2025**, *1037*, 182295. [CrossRef]
47. Fang, C.M.; Dinsdale, A.; Que, Z.P.; Fan, Z. Intrinsic defects in and electronic properties of θ-$Al_{13}Fe_4$: An ab initio DFT study. *J. Phys. Mater.* **2019**, *2*, 015004. [CrossRef]
48. Fang, C.M.; Que, Z.P.; Dinsdale, A.; Fan, Z. Si solution in θ-$Al_{13}Fe_4$ from first-principles. *Intermetallics* **2020**, *126*, 106939. [CrossRef]
49. Que, Z.P.; Fang, C.M.; Fan, Z. Nucleation competition and phase transformation mechanisms in recycled aluminium alloys: Insights into θ-$Al_{13}Fe_4$, Al_6(Fe,Mn) and α-Al_{15}(Fe,Mn)$_3Si_2$. *J. Alloys Compd.* **2025**, *1032*, 181130. [CrossRef]
50. Kresse, G.; Furthmüller, J. Efficiency of ab-initio total energy calculations for metals and semiconductors using a plane-wave basis set. *Comp. Mater. Sci.* **1996**, *6*, 15–50. [CrossRef]
51. Hohenberg, P.; Kohn, W. Inhomogeneous electron gas. *Phys. Rev. B* **1964**, *136*, B864–B871. [CrossRef]
52. Blöchl, P.E. Projector augmented-wave method. *Phys. Rev. B* **1994**, *50*, 17953–17978. [CrossRef]
53. Perdew, J.P.; Burke, K.; Ernzerhof, M. Generalized gradient approximation made simple. *Phys. Rev. Lett.* **1996**, *77*, 3865–3868. [CrossRef] [PubMed]
54. Fang, C.M.; van Huis, M.A.; Sluiter, M.H.F.; Zandbergen, H.W. Stability, structure and electronic properties of γ-$Fe_{23}C_6$ from first-principles theory. *Acta Mater.* **2010**, *58*, 2968. [CrossRef]
55. Monkhorst, H.J.; Pack, J.D. Special points for Brillouin-zone integrations. *Phys. Rev. B.* **1976**, *13*, 5188–5192. [CrossRef]
56. Arblaster, J. *Selected Values of the Crystallographic Properties of the Elements*; ASM International: Materials Park, OH, USA, 2018.
57. Pepperhoff, W.; Acet, M. The Magnetism of Iron, in: Constitution and Magnetism of Iron and its Alloys. In *Engineering Materials*; Springer: Berlin/Heidelberg, Germany, 2001.
58. Robinson, K.; Black, P.J. An X-ray examination of α(Al-Fe-Si) ternary compound. *Lond. Edinb. Dublin Philos. Mag. J. Sci.* **1953**, *44*, 1392–1397. [CrossRef]
59. Munson, D. A Clarification of the Phases Occurring in Aluminum-Rich Aluminum-Iron-Silicon Alloys with Particular Reference to the Ternary Phase α-AlFeSi. *J. Inst. Met.* **1967**, *95*, 217–219.
60. Li, X.L.; Scherf, A.; Heilmaier, M.; Stein, F. The Al-rich part of the Fe-Al phase diagram. *J. Phase Equilibria Diffus.* **2016**, *37*, 162–173. [CrossRef]
61. Asgar-Khan, M.; Medraj, M. Thermodynamic description of the Mg-Mn, Al-Mn and Mg-Al-Mn systems using the modified quasichemical model for liquid phases. *Mater. Trans.* **2009**, *50*, 1113–1122. [CrossRef]
62. Van Alboom, A.; Lemmens, B.; Breitbach, B.; De Grave, E.; Cottenier, S.; Verbeken, K. Multi-method identification and characterization of the intermetallic surface layers of hot-dip Al-coated steel: $FeAl_3$ or Fe_4Al_{13} and Fe_2Al_5 or Fe_2Al_{5+x}. *Surf. Coat. Technol.* **2017**, *324*, 419–428. [CrossRef]
63. Que, Z.P.; Wang, Y.; Mendis, C.L.; Fang, C.M.; Xia, J.H.; Zhou, X.R.; Fan, Z. Understanding of Fe-containing intermetallic compounds in Al-alloys: An overview of advanced in the LiME Research Hub. *Metals* **2022**, *12*, 1677. [CrossRef]
64. Shabestari, S.G.; Gruzleski, J.E. The Effect of Solidification Condition and Chemistry on the Formation and Morphology of Complex Intermetallic Compounds in Aluminium—Silicon Alloys. *Cast. Met.* **1994**, *6*, 217–224. [CrossRef]
65. Baker, I.; Cantor, B.; Yeh, J.W. High Entropy Alloys and Materials. *High Entropy Alloys Mater.* **2023**, *1*, 1–3. [CrossRef]
66. Wu, Q.; He, B.; Song, T.; Gao, J.; Shi, S.Q. Cluster expansion method and its application in computational materials science. *Comp. Mater. Sci.* **2016**, *125*, 243–254. [CrossRef]
67. Shurkin, P.; Scamans, G.; Subroto, T.; Barekar, N.; Sadeghi, F.; Nedreda, J.L.; Barbatti, C. Effect of Ti on microstructure and mechanical properties of high strength AA6xxx alloy. *Mater. Lett.* **2025**, *387*, 138280. [CrossRef]
68. Wu, Y.H.; Han, Y.; Zhang, J.S.; Zou, H.H.; Zu, G.Q.; Zhu, W.W.; Wang, W.; Ran, X. Achieving superior high-temperature strength-ductility in LPBF-processed aluminum matrix composite via in-situ oxide/intermetallic synergistically stabilizing Al-Si eutectic networks. *J. Manuf. Process.* **2026**, *172*, 1–13. [CrossRef]
69. Pichlmann, L.; Rafiezadeh, S.; Hofbauer, M.; Ocansey, E.D.; Österreicher, J.A. Predicting mechanical properties in aluminum alloys: A data-driven framework leveraging LLM-based data extraction and physics-based feature engineering. *Mater. Today Commun.* **2025**, *47*, 112843. [CrossRef]
70. Li, C.; Xian, Y.H.; Zhou, Y.M.; Ding, X.D.; Sun, J.; Xue, D.Z. Generative design for alloys: Harnessing generative models for faster discovery. *Adv. Mater.* **2026**, *38*, e20478. [CrossRef] [PubMed]